

Effect of Link-Beam Stiffener and Brace Flange Alignment on Inelastic Cyclic Behavior of Eccentrically Braced Frames

REZA IMANI and MICHEL BRUNEAU

ABSTRACT

Finite element analysis was used to investigate the effects of the misalignment of the brace flange-to-beam connection point with the link-end stiffener (referred to as the offset in the paper) on the ductility of eccentrically braced frames (EBF). The offset was speculated to be a possible reason for the unexpected EBF failures observed in the aftermath of the Christchurch earthquake series of 2010 and 2011. EBF models with different detailing at the offset area were analyzed under monotonic and cyclic displacements. Results showed severe stress and strain concentration in the offset area, preventing the EBF from developing its expected ductility, and suggested possible initiation of a failure from the part of link flange located in the offset area. Simulation using the ductile fracture model implemented in ABAQUS resulted in a fracture pattern in agreement with the actual failed EBF. Results from analyses on different detail configurations showed that removal of the offset by modifying the brace section to build an ideal case, or by a simple change in the location of the link stiffener, can mitigate the problem of possible premature failure, with the latter solution being slightly less effective but much easier to be used in practice.

Keywords: Eccentrically braced frames, EBF failure, eccentricity, offset at brace flange-to-beam connection.

INTRODUCTION

Previous analytical and experimental research has demonstrated that properly designed eccentrically braced frame (EBF) systems can provide the ductility and energy dissipation capacity needed to serve as an effective lateral load resisting system to resist earthquake demands (e.g., Roeder and Popov, 1978; Merovich et al., 1982; Hjelmstad and Popov, 1983; Malley and Popov, 1984; Kasai and Popov, 1986a, 1986b, 1986c; Ricles and Popov, 1987a, 1987b; Popov et al., 1987; Engelhardt and Popov, 1989a, 1989b). The EBF design requirements of the AISC *Seismic Provisions* (AISC, 2010b) are intended to concentrate the large inelastic deformations in EBFs subjected to seismic loading primarily into specially detailed ductile links. This will lead to cyclic yielding and energy dissipation in the link while all of the other members remain essentially elastic (AISC, 2010b).

While a number of EBF systems have been constructed around the world, EBFs were tested under an actual severe seismic event for the first time during the Christchurch earthquake series of 2010 and 2011. Reports from the aftermath of these events showed a relatively better performance

for steel structures compared to other structural systems (Bruneau et al., 2010; Clifton et al., 2011). The EBF systems that had been used in a few buildings in Christchurch generally exhibited a satisfactory behavior under the relatively intense shakings that occurred in the two largest earthquakes recorded during the 2010 and 2011 events. For instance, two multi-story buildings in the Christchurch central business district, which had EBFs as part of their lateral load resisting system, were green tagged and occupied after the earthquake series (Clifton et al., 2011), even though a life safety performance would be acceptable in seismic action of that intensity. However, some unexpected EBF link failures occurred during the 2011 event, including two in the EBF systems used in a parking garage in Christchurch's central business district. Those links typically exhibited a large fracture that had initiated in the link flange and progressed into the beam outside the link (Clifton et al., 2011).

Although the fracture, shown in Figure 1a, didn't jeopardize the overall performance of the building and the structure survived on account of the redundancy of the system (at least 6 EBF frames existed at the story where the link failure was observed), it remains that this is an undesirable behavior that has raised questions regarding the design and detailing of EBF systems to ensure development of their expected capacity and ductility. Clifton et al. (2011) speculated that this failure was possibly caused by a local stress concentration due to an offset between the brace flange-to-beam connection point and the link end-stiffener. The AISC *Seismic Provisions* require the use of full depth stiffeners at both

Reza Imani, Graduate Research Assistant, Department of CSEE, University at Buffalo, Amherst, NY (corresponding author). Email: rezaiman@buffalo.edu

Michel Bruneau, Professor, Department of CSEE, University at Buffalo, Amherst, NY. E-mail: bruneau@buffalo.edu

ends of all links to ensure the proper transfer of link shear forces to the reacting elements.

This paper reports the findings of a limited study conducted to investigate whether this eccentricity could have been the cause of the observed failures. Finite element analyses were used to investigate the cyclic inelastic behavior of EBF systems having different connection eccentricity details to identify the possible impact of such eccentricities, and recommend desirable configurations.

THE PROBLEMATIC CONNECTION DETAIL AND PROPOSED ALTERNATIVES

A closer look at the details of the connection in Figure 1a reveals that the brace flange was connected to the beam with an offset from the edge of the link stiffener. As indicated above, it was speculated that this eccentricity might have caused stress concentrations in that location, leading to a premature fracture in the beam flange in the offset area between the link stiffener and the brace flange, which then continued into the web of the beam outside the link. However, there were other EBF frames in the same building, which did not have the mentioned offset in the brace-to-beam connection and that showed a significant amount of yielding in the link without any fractures. Figure 1b shows one such link located in an upper story of the same structure, in which the link stiffener and the brace flange were vertically aligned.

Note that, according to a recent study on the two fractured EBFs by Marshall (2013), drawings of the details for the EBFs used in the parking garage showed a vertical alignment between the link stiffener and brace flange,

while the intersection of the beam and brace centerlines was located inside the link. The main reason for the occurrence of misalignment for some the EBFs in that building remains unknown to the authors. Because no fractures were seen in the other EBFs of the same building that had braces with flange connecting to the beams at a point more aligned with the link stiffener, circumstantial evidence seemed to support the conclusions of Clifton et al. (2011). However, quantifiable verification is desirable to more tangibly establish whether or not this issue was the possible cause of the observed fractures.

The reported EBF fractures were studied in a forensic examination by Kanvinde et al. (2012). Material samples were extracted from the fractured structures and subjected to Charpy-V notch toughness tests and tensile tests, to establish if potential deficiencies in material properties could explain the observed fractures. The material test results revealed satisfactory ductile behavior for the extracted coupons. A few finite element analyses on EBF models with detailing similar to the fractured structures were also conducted, showing stress concentrations at the eccentricity between the link stiffener and the brace flange.

The work reported here expands on the prior work by assessing the effect of brace flange alignment and work-line eccentricity on behavior of the connection. Four detail geometries, shown in Figure 2, were arbitrarily selected in this study and investigated using finite element analysis when subjected to monotonic and cyclic displacements.

Case EBF-1 is similar to the configuration used in the reported fractured EBFs, in that the stiffener is placed at the intersection of the brace and beam centerlines but doesn't vertically line up with the edge of the brace flange. This



Fig. 1. Photos of EBFs taken inside a parking garage following the Christchurch earthquake of 2011 (Clifton et al., 2011): (a) fractured EBF (lower level); (b) evidence of plastic action without fracture (top level).

geometry is selected as a generic case of an EBF with a wide flange brace directly welded to the beam, with the specific misalignment conditions mentioned above, and does not represent the exact geometry of the EBFs fractured in Christchurch. Analysis of one of those actual fractured EBF links, based on as-built dimensions, is presented in the last section of this paper.

The piece of the beam's bottom flange that is located between the link end-stiffener and the point where the flange of the brace is welded to the beam is referred to as the offset area from this point on in this report. Case EBF-2 represents the ideal configuration in which the stiffener is at the intersection of the beam and brace centerlines and the brace flange connects to the beam under the vertical stiffener (achieved by using a deeper brace member than the one in the previous case). The third case, EBF-3, is similar to EBF-1, except that the link end-stiffener has been moved to align vertically with the point where the flange of the brace is welded to the beam (as a consequence, the work-line of the brace intersects that of the beam inside the link, which is described as permitted in the Commentary to AISC 341-10. The last case, EBF-4, combines the misalignment of case EBF-1 with the situation where the work-lines of the beam and brace intersect outside the link; this last case, while not permitted by the 2005 AISC *Seismic Provisions* (AISC 341-05) was accepted into the 2010 version (AISC 341-10) with the condition that the beam outside the link must be designed for the subsequent additional moments (AISC, 2005; 2010b). This case is investigated out of curiosity, to determine if the effect of brace flange misalignment is compounded when the stiffener is not at the intersection of the brace and beam centerlines.

Two types of finite element analyses were conducted in this study. A first set of analyses examined the effects of the eccentricities mentioned above on the stress-strain distribution and deformations in the link and the elements close to the intersection of the brace and the beam. For the case where results showed critical stress and strain concentration, a second type of analysis was conducted to simulate the possible consequent path of fractures to compare with those occurred following the Christchurch earthquake.

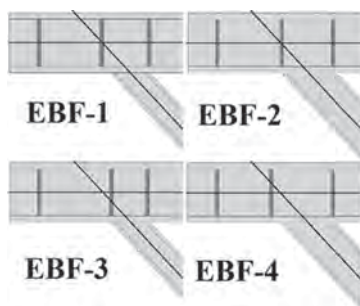


Fig. 2. Detailing alternatives for brace-to-beam connection.

FINITE ELEMENT MODELING

The general finite element software ABAQUS was used to study the behavior of EBF systems designed with different brace-to-beam connection details under monotonic and cyclic loading. Four models were built according to the design alternatives described above using approximately 100,000 linear 8-node 3D brick elements with reduced integration (i.e., element type C3D8R). Initial design parameters of the beam, column and brace were taken from a past experimental study on EBF frames (Berman and Bruneau, 2008) and were slightly modified to match the four cases mentioned above. All of the sections were modeled as wide-flange beams to resemble the conditions of the frame which fractured in the Christchurch earthquakes. Meshing strategy started with a uniform pattern for the whole model and was refined at the critical locations, after some preliminary analyses, to achieve more reliable results. Due to anti-symmetric condition of the system, only half of each frame was modeled with its corresponding connection detail.

A simple bilinear steel material with von Mises yield criteria was used for the beam, including the link. The material was defined with a uniaxial behavior that started with a linear elastic part with Young's modulus of 200,000 MPa (29,000 ksi) and yield stress of 350 MPa (50 ksi) at the strain value of 0.2%. The post-yield segment consisted of a linear strain hardening branch that continued up to the strength of 444.5 MPa (65 ksi) at the strain value of 15%. This resulted in a strain hardening slope equal to 3% of the initial stiffness. The column and the brace were set to remain elastic in all of the models throughout the analysis, because they were not expected to yield, and to accelerate execution time. Note that this assumption was validated by looking at the 3D state of stress in the column and brace members, which showed that their maximum von Mises stress values remained below the yield limit (these values were less than 50% of the yield in most of the cases).

Considering that no damage criteria were added to the model at this stage to simulate the behavior of the material from the point of maximum strength toward fracture, the uniaxial behavior of the steel material was defined to linearly lose its strength (from maximum to a value close to zero) over the strain range of 15% to 20%, while the latter was assumed to be the fracture strain. This configuration made it possible for the analysis to provide realistic results in terms of the strength of the frames, particularly at certain points throughout the analysis when a portion of element in the beam or the link had to go through severe plastic strains. The strain of 15%, which is corresponding to the von Mises stress value of 444.5 MPa, was defined as the limit beyond which the strength of the element starts to decline (onset of strength reduction), gradually making it ineffective in the overall behavior of the model. All four models were built with identical columns and beams, but with the

slight differences in stiffener positions and brace sections to implement the different connection details described earlier (Figure 2). Figure 3 shows two views of a typical built model.

The base of the column was modeled as a simply supported end as column deformations were not relevant for the plastic mechanisms studied. The nodes at the left of the beam were constrained to comply with the anti-symmetric boundary conditions (same horizontal translation and no vertical translation at the plane of symmetry). All of the members were modeled using the 8-node 3D solid elements. Monotonic or cyclic displacements were applied to the half frame by horizontally pushing and pulling the top of the column. Although the cyclic loading simulations were defined in the quasi-static mode (i.e., dynamic effects are not investigated in this study), the analyses were conducted using the dynamic explicit method, with appropriate considerations to avoid inertia effects, as it is a more effective approach to problems involving relatively high strains compared to the implicit method. All of the analyses were continued up to the point that severe deformations and distortions occurred at a number of elements in which the strain values surpassed the maximum limit defined above. After reaching this point, the strength loss and excessive distortions of the elements make it impossible for the analysis to continue.

RESULTS FROM FEM ANALYSIS ON DIFFERENT BRACE-TO-BEAM CONNECTION DETAILS

Push-over Analysis on EBF-1 Model (with Offset)

The main objective in the design of EBF systems is to concentrate the plastic action in the link while keeping the other parts, especially the beam outside the link, essentially elastic. Considering this design objective, plastic behavior of model EBF-1 was studied under push-over analysis to track the initiation and distribution of the plastic strains in different parts of the structure to identify possible failure

mechanisms. Because only half of the frame was modeled using anti-symmetric conditions in the middle of the link, two separate push-over analyses were conducted with displacements applied in opposite directions to check certain parts of the model for both tensile and compressive forces.

Figure 4 shows the graphs of base shear versus plastic link rotation for EBF-1 under monotonic applied displacements in two opposite directions. Both of the curves show significant strength loss at plastic link rotation values in the range 0.15 to 0.2 rad, which is expected for properly stiffened EBF frames. To distinguish the two opposite directions of applied displacements for push-over analyses, note that applying displacement in direction A causes tensile forces in the link bottom flange and applying displacement in direction B causes compression in the link bottom flange.

Considering the fact that the addition of a descending branch to the uniaxial behavior of the material can cause mesh-sensitive results for the elements which go beyond the maximum strength limit, push-over analysis for EBF-1 in direction B was repeated for a model with finer mesh. Mesh pattern 1 had elements with the approximate size of 10 mm fitting two elements along the thickness of the beam flange. Mesh pattern 2 was defined with elements half that size, with four elements across the thickness of the beam flange. Results from the two mesh patterns show the convergence of the finite element analyses for the different mesh sizes considered (Figure 4). The final mesh size was chosen such as to accommodate three elements across the thickness of the beam flange for all models to be used in the subsequent analyses in this study.

Results in Figure 4 show that EBF-1 loses strength at a relatively smaller plastic link rotation when monotonic loading is applied in the direction B. Loading in directions A and B creates positive and negative bending moments in the link, respectively. Significant loss of strength shows that a number of elements have surpassed the 15% strain limit (the onset of strength reduction) and are on the descending

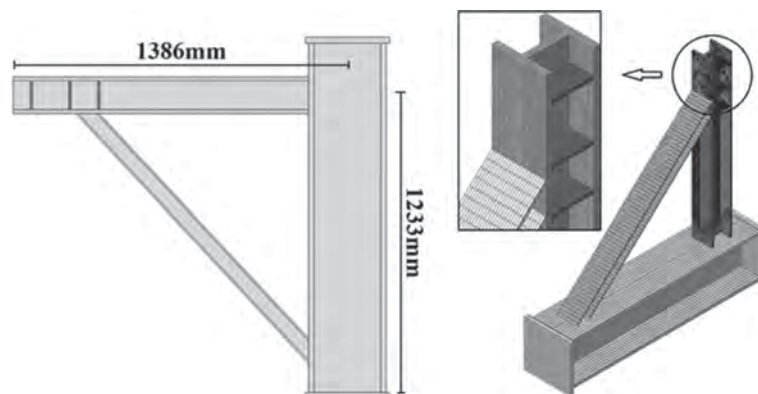


Fig. 3. Geometry and meshing of the finite element model.

branch of the stress-strain material model. To further investigate the differences between the location and strain response of the critical elements that cause the strength loss of EBF-1 under oppositely applied push-over loads, strain distribution and deformation plots were extracted from the ABAQUS analysis results for the two cases. Figure 5 shows the final deformed shapes of the EBF-1 half frame for both loading directions. Case A shows excessive deformations and element distortions in the web of the link close to one of the intermediate stiffeners leading to the strength loss of the structure. This type of behavior can be expected of EBF frames because the plastic action is intended to happen mostly in the link. On the other hand, case B shows excessive distortions for a different group of elements that

are located in the offset area, which can be considered as a sign of improper behavior based on the design objective of EBF systems.

The difference in the mechanisms leading to strength loss under loading from two opposite directions is due to the different stress and strain distribution that occurs in the offset area for the two cases. The relatively small piece of beam flange that is located between the link stiffener and the edge of the brace flange is under combined axial and shear forces that are applied in opposite directions for cases A and B (Figure 6). The onset of base shear loss seen in Figure 4 for cases A and B is when, having reached the von Mises yield surface and progressed to larger equivalent plastic strain values, the state of 3D stress in a number of elements in the

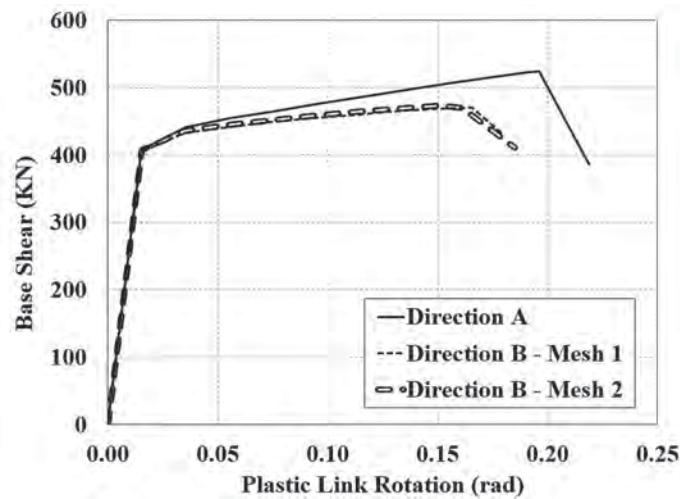


Fig. 4. Push-over analysis results for EBF-1 half frame under monotonic displacements in two opposite directions (plastic link rotation at the onset of base shear loss = 0.196 rad for case A and 0.161 rad for case B).

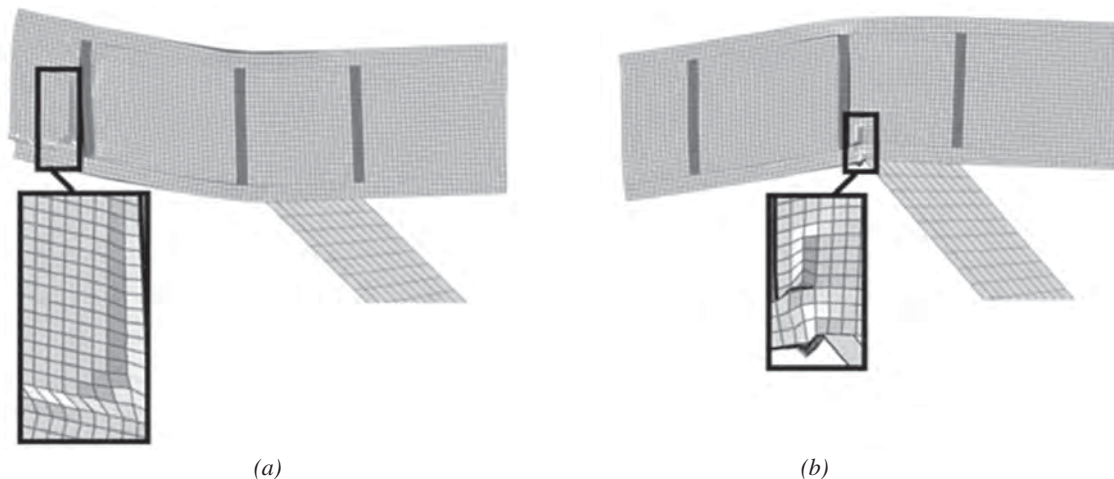


Fig. 5. Final deformation results from push-over analysis of EBF-1 in two opposite directions: (a) loading in direction A; (b) loading in direction B (plastic link rotation at the onset of base shear loss is 0.196 rad for case A and 0.161 rad for case B).

model reaches a point where their von Mises stress is equal to the maximum stress defined at the end of the strain hardening branch of the material's behavior (the stress of 444.5 MPa corresponding to the strain of 15% for the problem at hand). Any fraction of added plastic strain from this point on takes the elements into the stress declining branch, leading to strength reductions and element distortions seen in Figures 4 and 5.

Cases A and B reach this limit at different plastic link rotation values and, more importantly for the purposes of this study, for elements located in different parts of the EBF model. Figure 7 shows Mohr's diagrams for the 3D state of stress at the offset area for cases A and B. Stresses were calculated based on average values for 342 elements located

in the offset area at the onset of base shear loss. The figure shows that for case A, von Mises stress of the elements in the offset area have not reached the set maximum stress limit, and the drop in base shear was caused by the failure of a group of elements in the web of the link, as shown in Figure 5a. This is a preferred failure mode, as it allows development of yielding over the entire EBF link, prior to ultimately reaching strength degradation. For case B, on the other hand, the von Mises stress of the elements located in the offset area reached the set maximum stress limit, leading to a maximum shear stress on one of the principal planes equal to the corresponding maximum shear strength limit of the material ($\cong 0.57 \times 444.5 \cong 255$ MPa). Analogous to slip planes for yielding, attainment of the set shear strength limit

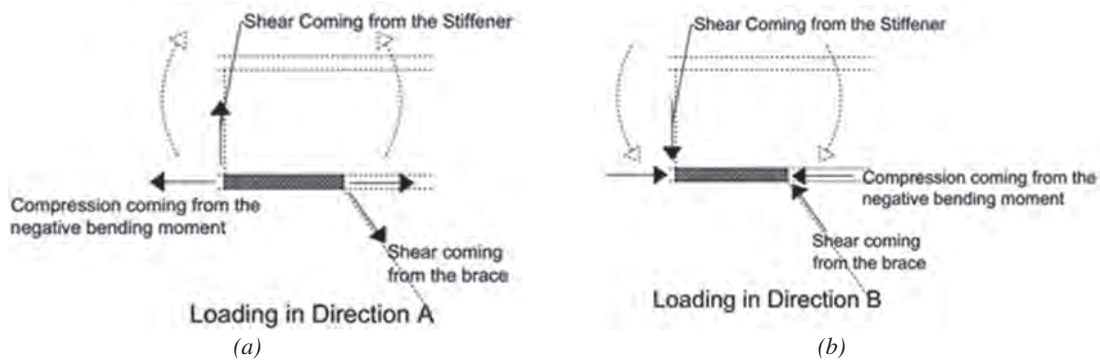


Fig. 6. Loads applied to the segment of the beam flange located at the offset: (a) loading in direction A; (b) loading in direction B.

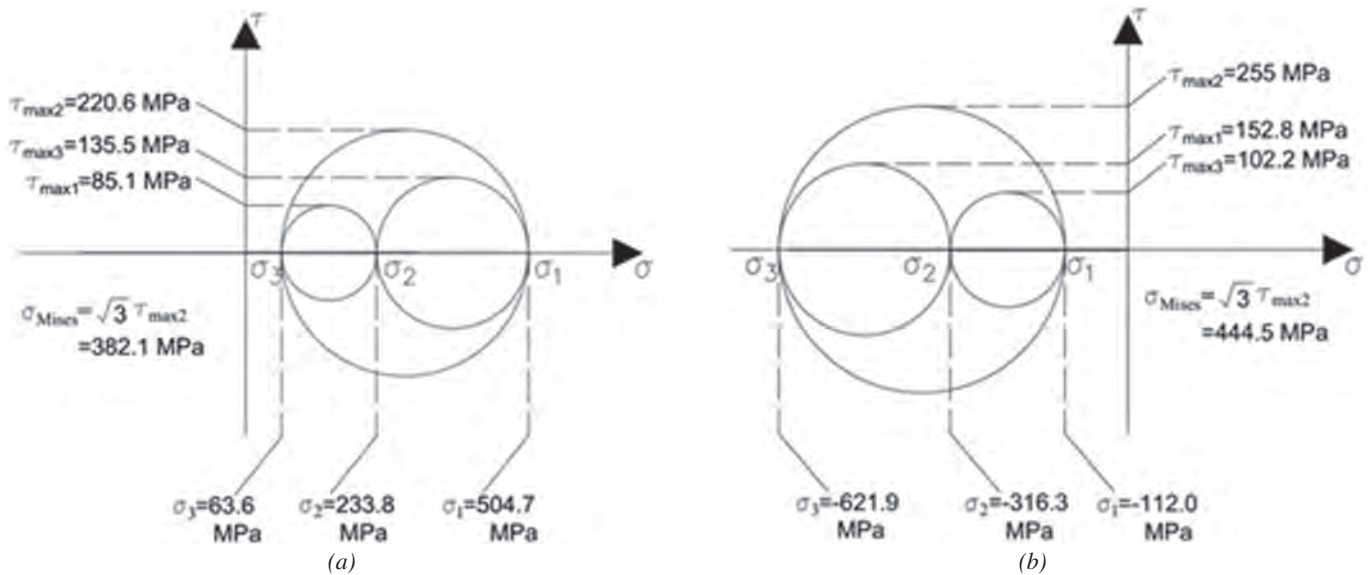


Fig. 7. Mohr's circle for 3D state of stress for elements in the offset area: (a) push-over loading in direction A; (b) push-over loading in direction B.

can be attributed to causing the possible onset of subsequent fracture. This assessment of stress conditions confirms that the failure of case B will start in the offset area.

The axial strain values (tensile for loading in direction A and compressive for loading in direction B) are plotted for a selected group of elements in the offset area versus the plastic link rotation values in Figure 8. The curves show that for case A the axial strain increases with the increasing plastic link rotation in the push-over analysis up to the point when the von Mises stress values for a number of elements in the web of the link reach the arbitrarily chosen maximum limit, causing the distortions shown in Figure 5a. From this point no more load is taken by the frame, and the axial strain remains constant for the elements in the offset area (excessive increase of plastic strains is limited to the distorted area in the web of the link). The scenario is different for case B, in which, as mentioned above, reaching the maximum stress level occurs in the beam flange at the offset area. This leads to an excessive increase in the average axial strain value for the selected group of elements in the offset area, as shown in Figure 8.

The equivalent plastic strain response parameter, $\bar{\epsilon}^{pl}$, provided by ABAQUS was used to identify the initiation and propagation of the potential fractures in the structure. The parameter integrates the combined effects of all the plastic strain components in the 3D space and gives the cumulative plastic strain for each element using the following equation:

$$\bar{\epsilon}^{pl} = \bar{\epsilon}_0^{pl} + \left(\sqrt{\frac{2}{3} \dot{\epsilon}^{pl} : \dot{\epsilon}^{pl}} \right) dt \quad (1)$$

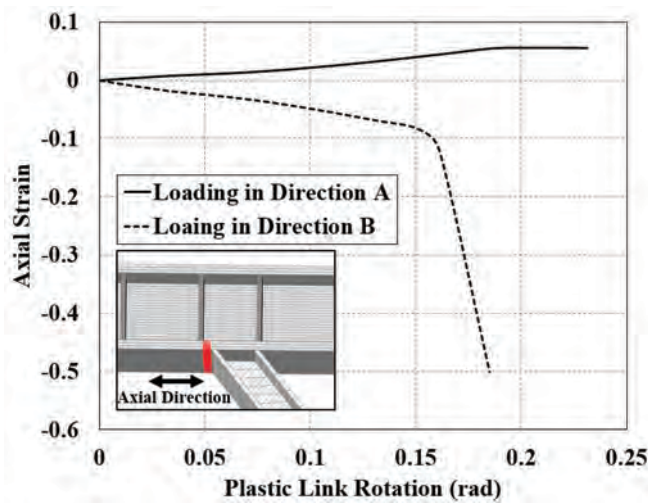


Fig. 8. Average axial strain values for a selected group of elements at the offset area from the push-over analysis of EBF-1 under loading in two opposite directions.

where $\bar{\epsilon}^{pl}$ is the initial equivalent plastic strain, which is set to zero for all the elements, and $\dot{\epsilon}^{pl}$ is the plastic strain rate tensor. According to the ABAQUS *Theory Manual*, the integration over time accumulates the incremental plastic strains of the elements throughout the analysis (Simulia, 2012). Based on the material behavior defined for the beam (including the link), an equivalent plastic strain equal to 19.8% for any element in the models built in this study means that it has reached the fracture strain limit (total strain of 20%, considering the elastic strain limit of 0.2%). Going past this limit, the element will continue to experience higher plastic strain values without contributing to the strength or resistance of the structure.

Figure 9 shows the distribution of equivalent plastic strain for EBF-1 under monotonic loading in two opposite directions. The contours are plotted on the undeformed shapes to get a clearer picture of the equivalent plastic strain distribution. Locations with $\bar{\epsilon}_0^{pl}$ values above 19.8% (areas shaded in gray) can be considered as those having exceeded the fracture initiation points. Results show that the elements reaching the fracture plastic strain limits are located at the web of the link for the frame loaded in direction A and at the offset area for the frame loaded in direction B (as indicated previously, in Figure 5). The color contours for EBF-1 loaded in direction B suggest that a fracture may initiate in the beam flange and propagate further into the beam outside the link, following a pattern that resemble the one reported for the EBF damaged during the Christchurch 2011 earthquake.

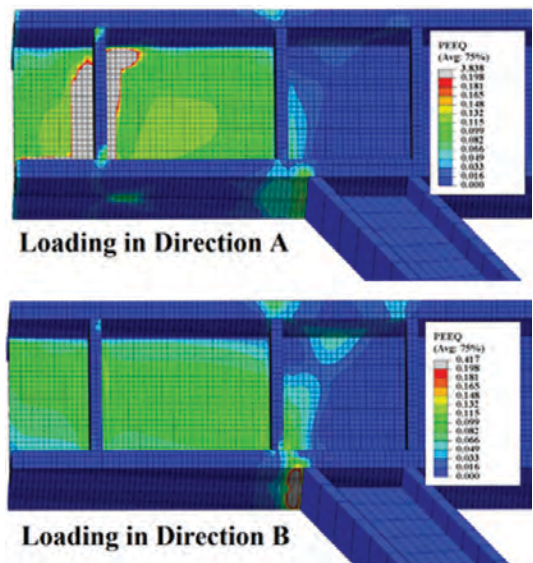


Fig. 9. Equivalent plastic strain distribution for EBF-1 under monotonic loading in two opposite directions (plastic link rotation at the onset of base shear loss is 0.196 rad for case A and 0.161 rad for case B).

Push-over Analysis on EBF-2 Model (without Offset)

To further examine the effects of the mentioned detailing issue on the static behavior of the EBF frames, model EBF-2 was subjected to a push-over analysis for displacements in direction B, which puts the bottom flange of the link in compression. Recall that in EBF-2, the brace flange connection point to beam lines up vertically with the link stiffener, which is located at the intersection of the centerlines of the beam and the brace.

Figure 10 shows the final deformed shape of EBF-2 after the occurrence of excessive distortions, along with the equivalent plastic strain distribution for the elements plotted on the undeformed shape of the frame. Results show that, when subjected to a push-over loading conditions similarly to case B discussed above for EBF-1, the average von Mises stress values for the elements in the beam to brace flange connection point (close to the link stiffener), did not reach the maximum stress limit (and onset of strength loss) until

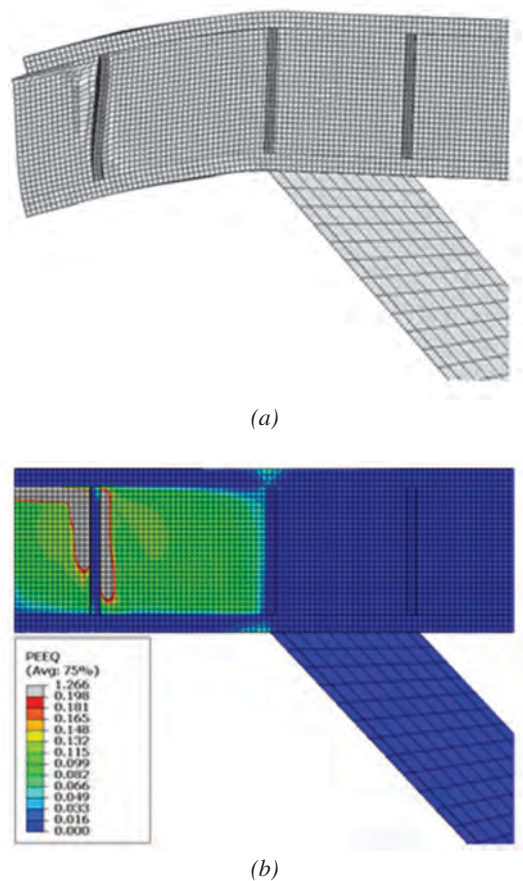


Fig. 10. Results from push-over analysis of EBF-2 with bottom flange of the link in compression after occurrence of excessive element distortions: (a) final deformed shape; (b) distribution of equivalent plastic strains on all elements (plastic link rotation at the onset of base shear loss = 0.27 rad).

the frame started to lose base shear strength because a number of elements located in the web of the link reached the maximum stress limit at the plastic link rotation of 0.27 rad, which is significantly larger than the onset of base shear strength loss for EBF-1 (i.e., 0.161 rad for case B). Thus, results show that proper alignment of the brace flange with the link stiffener (which was located at the intersection of the beam and brace centerlines) transferred the plastic action into the link, preventing the occurrence of yielding (and subsequently reaching the maximum stress level) in the brace-to-beam connection area.

Comparison of results in Figures 9 and 10 highlights the possible impact on behavior caused by slight differences in the detailing of the brace-to-beam connection, and how location of the link stiffener with respect to these two members can affect the ultimate inelastic behavior of the EBF frame. Under similar push-over analysis conditions, EBF-2 developed a maximum plastic link rotation of 0.27 rad and all significant plastic behavior concentrated in the link, whereas EBF-1 lost resistance at the significantly smaller plastic link rotation of 0.16 rad and developed substantial plastic behavior in the offset area (average stress values reached the maximum defined value).

Cyclic Analysis on Models with All Four Detailing Alternatives

To further investigate whether the stress concentration observed above can have an impact on the seismic performance of links, the four detailing configurations shown in Figure 2 were subjected to cyclic lateral loading. Although low-cycle fatigue is not considered in this study, cyclic loading was applied to the models because cumulative cyclic inelastic deformations in load reversals can induce imperfections in the structure. These imperfections can generally lead to total strength losses and element distortions, which, for the models studied here, is equivalent to reaching to the arbitrarily chosen maximum stress or its corresponding maximum strain limit, at smaller lateral displacements than those predicted under monotonic loading conditions.

Cyclic lateral displacements were applied to all models to create the plastic link rotation cycles shown in Figure 11. The arbitrarily selected displacement protocol consists of inelastic cycles creating different amplitudes of plastic link rotation of the EBF frames. Starting with a plastic rotation of 0.025 rad, it increases in two steps up to 0.08 rad and stops at rotation of 0.06 rad during the final unloading segment. Actual maximum plastic link rotation was slightly above or below the 0.08 rad limit for some of the models considered because the link's geometry was changed slightly for the different models, but the same lateral displacements were applied to all models. As mentioned before, because low-cycle fatigue issues were not considered in this study, and for computational expediency, just a few inelastic

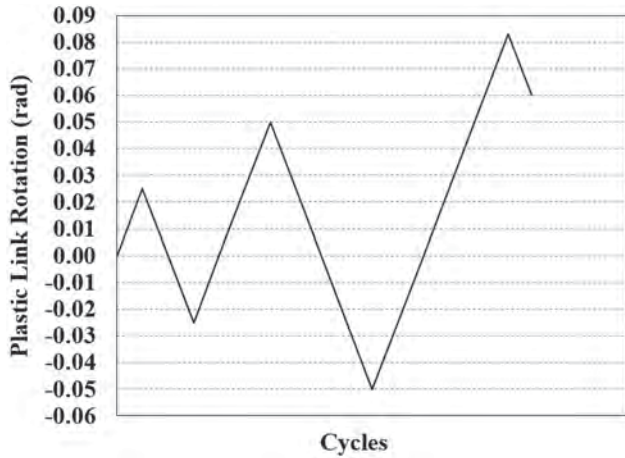


Fig. 11. Cyclic lateral loading protocol applied to the models.

cycles were applied to the structure to create imperfections, avoiding replicating the type of cyclic displacement protocols typically done in experimental studies (as this would have required substantially longer computational time). The arbitrarily chosen maximum equivalent plastic strain limit of 19.8% (used for push-over analysis) was kept as the limit for the cumulative plastic strain in the cyclic analyses. This limit was chosen to provide a uniform basis of comparison for all models while limiting analysis to a small number of cycles (for computational expediency), recognizing that a significantly higher limit would have to be used if the models were analyzed under the full AISC loading protocol to consider the qualification of EBFs (which is not necessary here, for the purpose of the current study).

Figure 12 shows the resulting base shear versus plastic link rotation values from cyclic analyses for all four models.

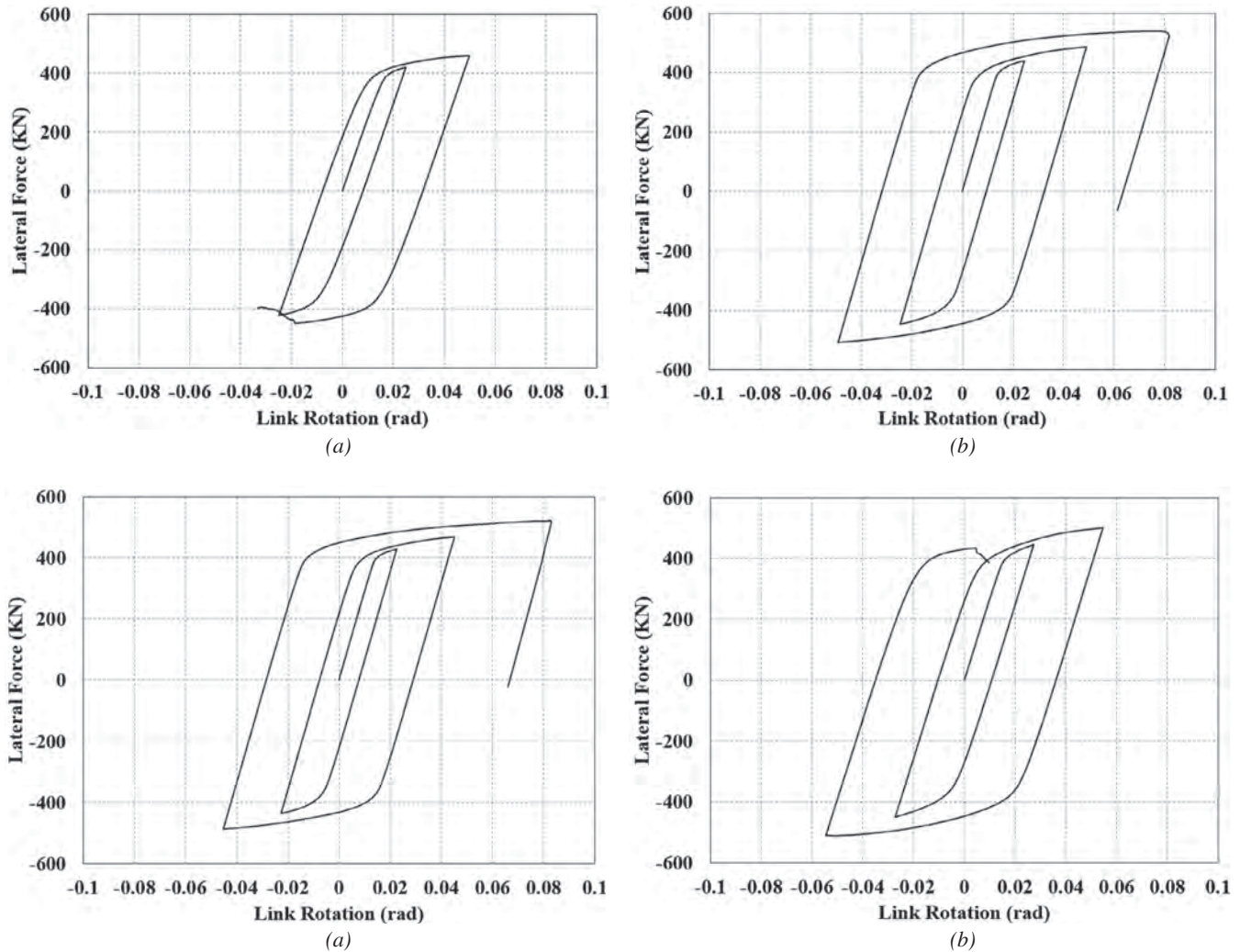


Fig. 12. Base shear versus plastic link rotation results from cyclic analyses: (a) EBF-1; (b) EBF-2; (c) EBF-3; (d) EBF-4.

Analysis of model EBF-1 terminated due to high compressive strains and element distortions in the offset area, similarly to what was observed in the push-over analysis but at a relatively smaller plastic link rotation value (0.03 rad for cyclic analysis as opposed to 0.16 rad for the monotonic one). The difference is due to the fact that equivalent plastic strain for the elements in the offset area reaches the defined maximum limit (19.8%) much sooner in the cyclic analysis because of the accumulation of plastic strain during the cycles. Because plastic action is concentrated in the offset area rather than being distributed in the whole link, the accumulated plastic strain values reach the maximum limit in a few cycles.

EBF-2 exceeded the plastic link rotation of 0.08 rad without problem, showing the effectiveness of the adjustment made to the connection. The removal of the offset has transferred the plastic action into the link, preventing the elements at the connection point from reaching the maximum limit of the equivalent plastic strain. Interestingly, EBF-3 also exceeded the 0.08 rad plastic link rotation, which supports the AISC 341-10 recommendation, provided that the link stiffener lines up with the point where the brace's flange connects to the beam flange. This result shows that if the geometry of EBF-2 cannot be accomplished (due to limits in available brace depths), satisfactory ductile behavior of the frame can still be ensured by locating the stiffener such as to eliminate the stiffener-to-brace flange offset.

Finally, while EBF-4 resisted two complete cycles (i.e., exhibiting a ductile behavior better than EBF-1), it lost strength at the beginning of the third cycle in a pattern similar to that of EBF-1 in the offset area. However, better performance of EBF-4 suggests that it has been more effective in distributing the plastic action into the link compared to EBF-1. To further investigate this issue and overall differences in the behaviors of the four detailing alternatives considered here, contours of equivalent plastic strain, $\bar{\epsilon}^{pl}$, were plotted on the undeformed shapes of the models at the final stages of their analyses (Figure 13). The analysis for each model was terminated either because of the completion of the displacement protocol (for EBF-2, 3) or because of significant strength loss and element distortions in the model (for EBF-1, 4). The latter occurred when a number of elements surpassed the maximum plastic strain limit (19.8%), which led to their severe distortions. The plastic link rotation values for all models at the analysis termination points can be determined from the ends of the curves plotted in Figure 12.

The orientation of the equivalent plastic strain contour lines in Figure 13 suggests (in ideal conditions) probable failure patterns that may occur once strains have reached extreme values. However, it is recognized that the ultimate

failure mode of EBF links may also be affected by a number of other factors not considered here, such as triaxial residual stresses and micro-defects introduced during welding of the stiffeners, which may impact low-cycle fatigue life.

The plots in Figure 13 show that models EBF-1 and EBF-4 will have a failure at the offset between the link stiffener and the brace flange similar to what was seen following the Christchurch earthquake series. The stress contours reveal that the elements of the link for EBF-4 have equivalent plastic strain values in the range of 0.10 to 0.13 rad, which is considerably higher than the values for the link elements of EBF-1 (0.02 to 0.06 rad). The difference shows the more effective distribution of plastic action in the link of EBF-4 as the main reason for its better performance with respect to EBF-1. It should be mentioned that a closer look at the arbitrarily selected geometry of EBF-4 (Figure 2) reveals that the intersection of beam and brace centerlines (located outside the link) almost lines up vertically with the brace flange to beam connection point, although the stiffener is moved away to create the offset. This might be one possible reason for the EBF-4's being more effective in transferring the plastic action toward the link, as compared to EBF-1. Note that this is just a suggested interpretation of the simulation results and that, at any rate, a detailing similar to EBF-4 is unlikely to occur in real cases.

Model EBF-2 has experienced its maximum equivalent plastic strain value in the web of the link close to the intermediate stiffener. The contour colors show that if the applied displacement protocol was extended to continue the analysis, the first group of elements surpassing the fracture plastic strain limit would be located in the same area as expected of EBF systems. EBF-3 shows an acceptable ductile behavior by transferring the plastic action to the link and surviving during the applied displacement protocol. Although EBF-3 seems like an easier solution to implement than EBF-2 to eliminate the offset problem, the orientation of the contour lines and their colors, which are plotted at the same stage of analysis for both models (i.e., at the end of the displacement protocol, when plastic link rotation have reached 0.06 rad), show the possibility of a more premature failure for EBF-3 compared to the ideal case EBF-2. Figure 13 suggests that the possible fracture of EBF-3 may start in the link flange, close to its meeting point with the brace flange, and progress in a path toward the intersection of the link and brace centerlines. It appears that although moving the stiffener to line up with the brace flange has eliminated the offset for EBF-3 leading to an acceptable behavior, it may still ultimately fail by a fracture starting in the link flange (rather than in the web of the link) if higher displacement amplitudes are applied. Considering the plots of Figure 13 altogether, EBF-2 shows the best behavior among the four alternatives.

SIMULATION OF THE POTENTIAL FRACTURE IN EBF SYSTEMS

In the above nonlinear inelastic finite element analyses, average equivalent plastic strain values were calculated, and elements with strain values exceeding the specified fracture limit of the material were deemed to have failed (even though the elements remained part of the continuum). While the resulting strain contours displayed zones of largest strains near the region where actual fracture was observed in Christchurch for a similar configuration (EBF-1), it is

worthwhile to further investigate the behavior of that specific case using the damage model for ductile materials available in ABAQUS. This model can simulate fracture propagation in the EBF-1 frame by automatically deleting elements that reach a full-damage criterion during the analysis. Moreover, because the damage evolution capability used in the ABAQUS model degrades the element stiffness based on plastic displacements and fracture energy measures rather than just plastic strain, it can generally provide reasonable accuracy in replicating fracture propagation, although it is recognized that exact matching of a fracture

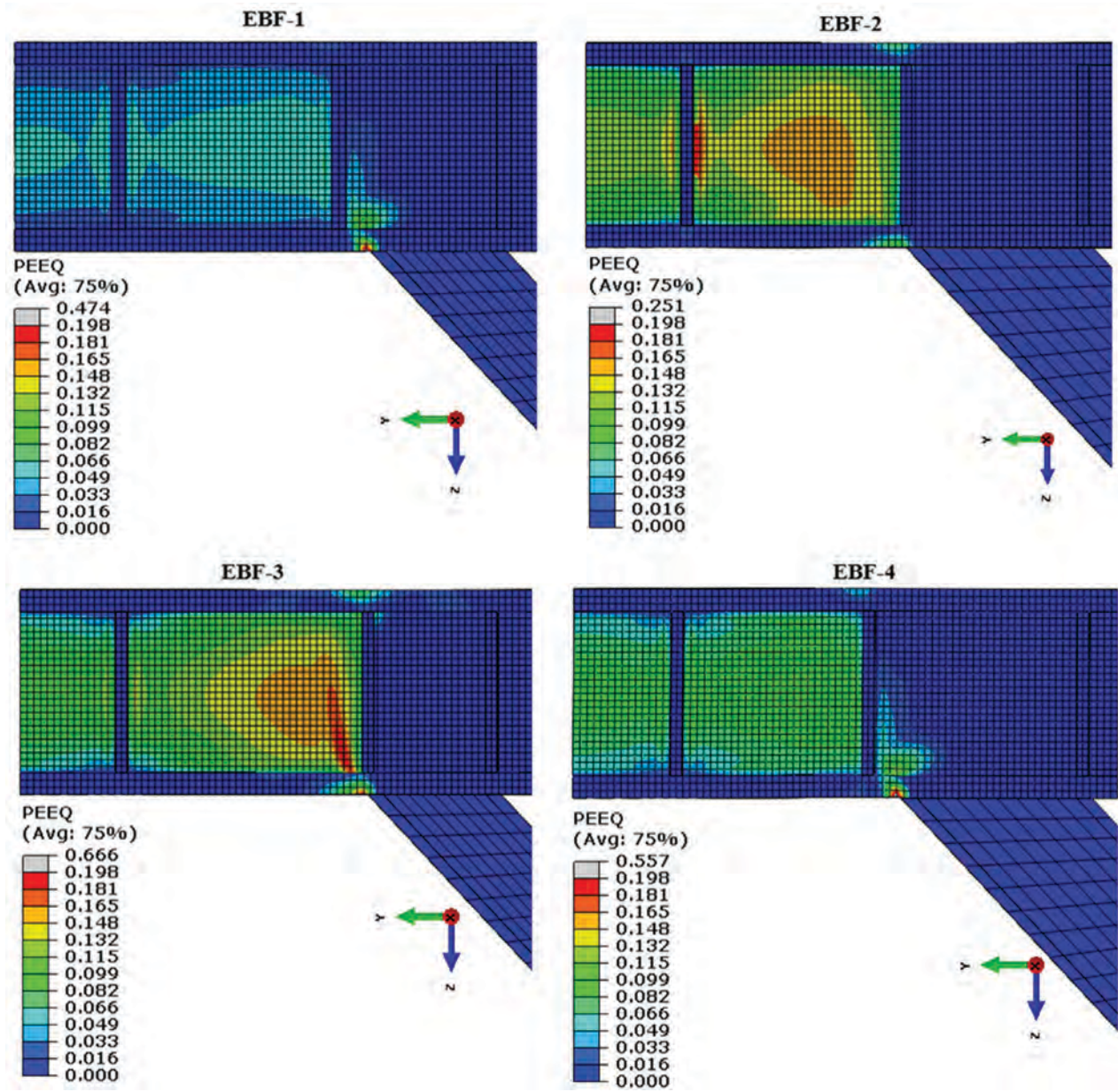


Fig. 13. Distribution of equivalent plastic strain values for all four models close to their failure under cyclic loading.

path may be difficult. The purpose is not to obtain perfect replication of the progression and path of the fracture, but to get a preliminary indication of how it could propagate after its initiation. Note that achieving a perfect replication of the fracture propagation path would need the implementation of an adaptive step-by-step mesh refinement strategy at the crack tip, similarly, for example, to what was done in a study by Roy and Dodds (2001) on the simulation of ductile crack growth in thin aluminum panels—but such a level of refinement was beyond the of scope of this study.

This type of material modeling, to predict the onset of damage and model the progressive damage and failure of ductile metals, requires three main properties: the elastic-plastic behavior of the undamaged material, a damage initiation criterion and a damage evolution response that can include the criteria for removal of failed elements. The specifics of the damage simulation model for ductile metals used in this investigation are summarized in the following paragraphs (Simulia, 2012).

The ductile fracture criterion was used as the damage initiation model in this study. The model assumes that the equivalent plastic strain at the onset of damage, $\bar{\epsilon}_D^{pl}$, can be defined as a function of stress triaxiality and strain rate:

$$\bar{\epsilon}_D^{pl} = f(\eta, \dot{\bar{\epsilon}}^{pl}) \quad (2)$$

where $\eta = -p/q$ is the stress triaxiality, p is the pressure stress, q is the von Mises equivalent stress, and $\dot{\bar{\epsilon}}^{pl}$ is the equivalent plastic strain rate. A state variable, ω_D , is defined

by Equation 3 and increases monotonically with plastic deformation with incremental steps that are calculated by Equation 4 for each increment of the analysis. The damage initiation criterion is met when the condition $\omega_D = 1$ is satisfied.

$$\omega_D = \int \frac{d\bar{\epsilon}^{pl}}{\bar{\epsilon}_D^{pl}} \quad (3)$$

$$\omega_D = \frac{\bar{\epsilon}^{pl}}{\bar{\epsilon}_D^{pl}} \quad (4)$$

The damage evolution capability in this model works by progressive degradation of material stiffness leading to its failure. The model is based on mesh-independent measures, including plastic displacements and energy dissipation, to simulate the damage evolution of the material after the damage initiation. Figure 14 shows the stress-strain curve for a material with progressive damage degradation, where $\sigma_{y0}, \bar{\epsilon}_0^{pl}$ are the yield stress and equivalent plastic strain at the onset of the damage and $\bar{\epsilon}_f^{pl}$ is the equivalent plastic strain at failure when the overall damage variable reaches its maximum value ($D = 1$).

Because the value of $\bar{\epsilon}_f^{pl}$ depends on the characteristic length of the element, L , which is a mesh dependent parameter, the damage evolution law is either based on the equivalent plastic displacement, \bar{u}^{pl} , or fracture energy dissipation, G_f .

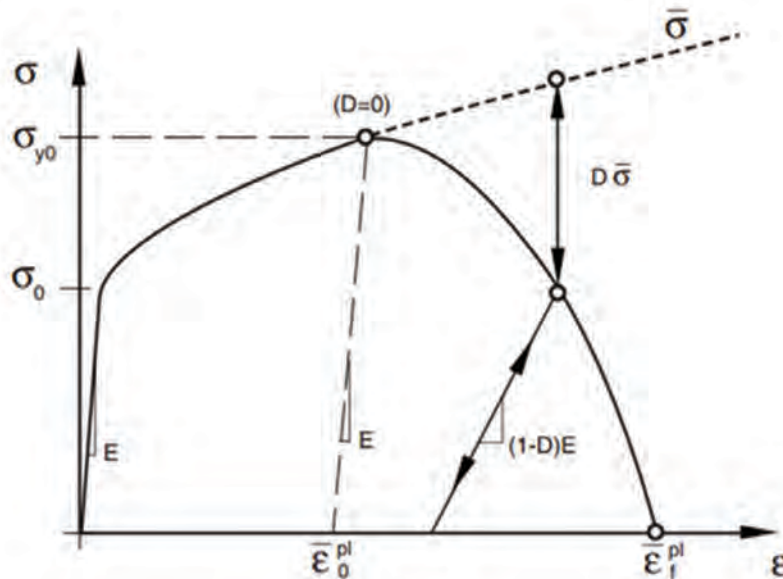


Fig. 14. Stress-strain curve for material with progressive damage degradation (Simulia, 2012).

$$G_f = \int_{\bar{\epsilon}_0^{pl}}^{\bar{\epsilon}_f^{pl}} L \sigma_y d\bar{\epsilon}^{pl} = \int_0^{\bar{u}_f^{pl}} \sigma_y d\bar{u}^{pl} \quad (5)$$

The fracture energy is calculated based on the characteristic length of each element according to Equation 5. The definition of the characteristic length, L , depends on the geometry and formulation of the element. It is defined as the length of a line across a first order element, or half of same length for second-order elements. Equation 5 also introduces the definition of the equivalent plastic displacement, \bar{u}^{pl} , which has the change rates of $\dot{\bar{u}}^{pl} = 0$ before damage initiation and $\dot{\bar{u}}^{pl} = L \dot{\bar{\epsilon}}^{pl}$ after it. At any given time during the analysis the stress tensor is given by:

$$\sigma = (1 - D) \bar{\sigma} \quad (6)$$

where D is the overall damage variable and $\bar{\sigma}$ is the effective (undamaged) stress tensor computed in the current increment. ABAQUS can be set up to remove the elements that reach the limit $D = 1$.

For these analyses, damage initiation was set up to start at the equivalent plastic strain of 0.15 for the beam of EBF-1 model (including the link). Damage evolution was defined based on the equivalent plastic displacement with a linear softening that would reach failure at the equivalent plastic displacement calculated using the characteristic length of 5 mm (from the mesh size) and failure plastic strain of 19.8%. ($\bar{u}_f^{pl} = L \bar{\epsilon}_f^{pl}$). The element deletion option was also used to remove the elements that reach the failure criterion. EBF-1 was subjected to cyclic lateral displacements for fracture simulation. The mesh size with three elements along the thickness of the beam flange, which was shown to be fine enough based on the mesh sensitivity analysis check mentioned above, was used in an attempt to predict the direction of the fracture at the offset area.

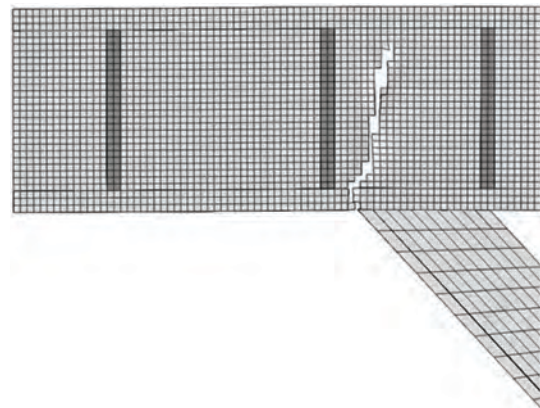
Figure 15 shows plots of the resulting simulated fracture in the EBF-1 model with and without the equivalent plastic strain contour lines. The simulated fracture initiated at almost the same location as the one reported from the Christchurch earthquake (Figure 1a) and progressed into the web of the beam outside the link. However, due to the mesh dependency of the fracture growth path and the fact the simulated fracture growth could only occur along the element edges, the simulated fracture progresses in a relatively more vertical path compared to the one occurred in the Christchurch earthquake. The problems of mesh size and mesh orientation sensitivity for fracture simulation can be resolved by using an adaptive mesh refinement strategy, where the new topology around the crack tip goes through mesh refinement for the next step of the analysis (similar to the study mentioned above by Roy and Dodds). However, using such computational techniques was beyond the scope of this study. Note that the fracture also follows a path similar to what was predicted from the equivalent plastic strain

distribution contours in Figure 9 obtained from the static push-over analysis of EBF-1 with the link's bottom flange in compression. Contour line colors reveal that most of the plastic behavior is concentrated in the offset area with a limited yielding in the link (which is consistent with slight flaking of the paint seen in the link of the fractured EBF shown in Figure 1).

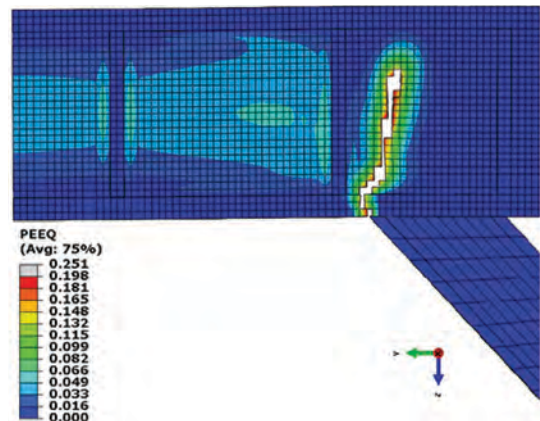
CASE STUDY

Push-over Analysis of a Model Built Using the As-Constructed Dimensions and Details of the EBF Frame Fractured in Christchurch

Considering the problematic effects of the offset in the brace-to-beam connection area on the overall behavior of EBF frames (as demonstrated above), an additional finite element model was built using the as-constructed dimensions and details of one of the EBF frames that was reported



(a)



(b)

Fig. 15. Simulated fracture at the offset between the link stiffener and the brace flange of EBF-1 (with and without the equivalent plastic strain contour lines).

to have fractured during the Christchurch earthquake series. This model is referred to as EBF-5 from this point on in this paper. The dimensions of the members (i.e., 460UB67 and 250UC73 sections for the beam and brace) were adopted from a recent study on these fractures (Marshall, 2013) and the model was built as a complete frame to account for the fact the offset was only observed on one side of the fractured frame. Push-over analyses were conducted in two opposite directions and the results of equivalent plastic strain distribution at the onset of base shear loss is shown in Figure 16.

Figure 16a shows that for push-over loading in direction A (i.e., offset area in compression), considerable plastic action has occurred in the link, while the flange of the beam in the offset area remains well below the 15% equivalent plastic strain limit; in other words, no strength loss has occurred for the elements of the beam flange in the offset area when the elements in the link reached the onset of strength loss. Loading in direction B (i.e., offset area in tension), on the other hand, has caused a significant plastic strain concentration in the elements of the beam flange in the offset area, which can be considered as a possible premature fracture initiation point (Figure 16b). Note that this situation is somewhat different than what had been observed previously for push-over of EBF-1 (discussed above), as the critical stresses in the offset occur in tension rather than compression. The difference is due to the fact that EBF-5 has a much thinner and more flexible beam flange, and most of the compression load, when the frame is pushed in direction A, is sustained by the web of the beam. Note that no such strain concentration occurred on the right side of the link where brace flange aligned with the link end stiffener.

Even though loading in direction B has the more critical equivalent plastic strain distribution, the offset area can also be considered to cause problems for the frame when loading is applied in direction A. Overall, the behavior of EBF-5 under push-over loading underscored the possibility of the occurrence of premature EBF fractures due to the stress and strain concentrations in the offset area.

Incidentally, it was suspected that, for the specific case of the Christchurch EBF, local web yielding in the beam in the offset area might have increased the demand in the beam flange, thereby leading to a possible subsequent fracture. To verify this, a simple check of the 2010 AISC *Specification* criteria (Specification Equation J10-2) for local web yielding under concentrated loads was performed using the vertical component of the load in the brace flange connected to the beam in the offset area (calculated from the finite element analysis results). Calculations showed that the concentrated load applied by the brace flange was about 70% of the available strength provided per AISC *Specification* Equation J10-2. It was inferred that local web yielding in the beam could not be the main reason for the fracture initiation.

CONCLUSION

Four eccentrically braced frames having different locations for their link stiffeners with respect to the beam-to-brace flange connection point and intersection of brace-to-beam centerlines were analyzed using the finite element method to investigate their potential vulnerabilities and possibly explain some of the fractures reported following the Christchurch earthquake series of 2010 and 2011.

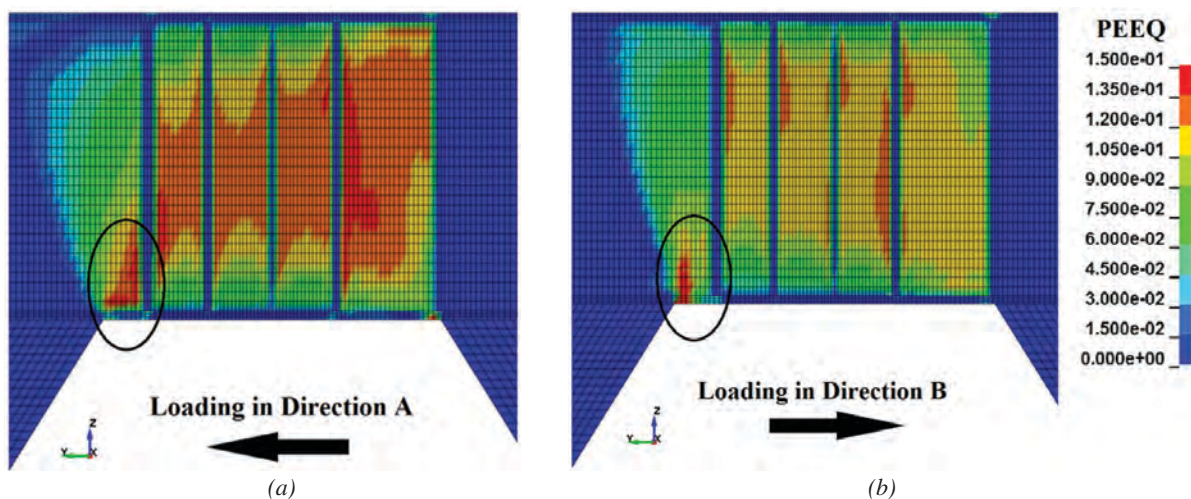


Fig. 16. Distribution of equivalent plastic strains at the onset of base shear loss for EBF-5 subjected to push-over loading in (a) direction A (plastic link rotation = 0.23 rad); (b) direction B (plastic link rotation = 0.18 rad).

Results from limited monotonic and cyclic analyses, as well as from analyses considering fracture propagation based on the use of damage models, combine to demonstrate that the eccentricity (misalignment) of link stiffeners with respect to the beam-to-brace flange connection point is responsible for the observed premature failures outside of the link. This is attributed to the severe stress concentration condition that develops in that area. The conditions leading to such failures were not observed to develop in absence of this eccentricity.

Modifying the section of the brace to achieve a condition in which the intersection of the beam and brace centerlines line up vertically with the edge of the brace flange as well as with the link-end stiffener was shown to be effective in solving the potential fracture problem by properly transferring the plastic action into the link. For cases where modifying the brace section to achieve the above condition is not possible, analyses showed that simply moving the link stiffener to eliminate the offset between the end stiffener and beam-to-brace flange connection point is almost as effective to improve the overall behavior of the EBF frame, even if the intersection of brace-to-beam centerlines falls inside the link. Note that the results of this study are limited to EBF frames with wide flange braces, as all of the simulation models were built with that configuration. Even though it is likely that the existence of the offset might cause similar problems for frames in which other types of brace sections and connections are used, the distribution of the plastic strains and subsequent damage might be different for those cases and needs further investigation.

REFERENCES

- AISC (2005), ANSI/AISC 341-05, *Seismic Provisions for Structural Buildings*, American Institute of Steel Construction, Chicago, IL.
- AISC (2010a), ANSI/AISC 360-10, *Specification for Structural Steel Buildings*, American Institute of Steel Construction, Chicago, IL.
- AISC (2010b), ANSI/AISC 341-10, *Seismic Provisions for Structural Steel Buildings*, American Institute of Steel Construction, Chicago, IL.
- Berman, J. and Bruneau, M. (2008), "Tubular Links for Eccentrically Braced Frames. II: Experimental Verification," *Journal of Structural Engineering*, ASCE, Vol. 134, No. 5, pp. 692–701.
- Bruneau, M., Anagnostopoulou, M., MacRae, G., Clifton, C. and Fussell, A. (2010), "Preliminary Report on Steel Building Damage from the Darfield (New Zealand) Earthquake of September 4, 2010," *New Zealand Society for Earthquake Engineering Bulletin*, Vol. 43, No. 4, pp. 351–359.
- Clifton, C., Bruneau, M., MacRae, G., Leon, R. and Fussell, A., (2011), "Steel Structures Damage from the Christchurch Earthquake of February 22, 2011, NZST," *Bulletin of the New Zealand Society for Earthquake Engineering*, Vol. 44, No. 4, pp. 297–318.
- Engelhardt, M.D. and Popov, E.P. (1989a), "On Design of Eccentrically Braced Frames," *Earthquake Spectra*, Vol. 5, No. 3, pp. 495–511.
- Engelhardt, M.D. and Popov, E.P. (1989b), "Behavior of Long Links in Eccentrically Braced Frames," *Report: UCB/EERC-89/01*, California University, Richmond. Earthquake Engineering Research Center, Sponsor: National Science Foundation, Washington, DC.; American Iron and Steel Institute, Washington, DC, 415p, January, 1989.
- Hjelmstad, K.D. and Popov, E.P. (1983), "Cyclic Behavior and Design of Link Beams," *Journal of Structural Engineering*, Vol. 109, No. 10, pp. 2387–2403.
- Kanvinde, A.M., Grilli, D.A. and Marshall, K. (2012), "A Framework for Forensic Examination of Earthquake Induced Steel Fracture Based on the Field Failures in the 2011 Christchurch Earthquake," *Proceedings of Fifteenth World Conference on Earthquake Engineering*, Lisbon, Portugal.
- Kasai, K. and Popov, E.P. (1986a), "General Behavior of WF Steel Shear Link Beams," *Journal of Structural Engineering*, ASCE, Vol. 112, No. 2, pp. 362–382.
- Kasai, K. and Popov, E.P. (1986b), "Cyclic Web Buckling Control for Shear Link Beams," *Journal of Structural Engineering*, ASCE, Vol. 112, No. 3, pp. 505–523.
- Kasai, K. and Popov, E.P. (1986c), "Study of Seismically Resistant Eccentrically Braced Steel Frame Systems," *Report: UCB/EERC-86/01*, California University, Richmond. Earthquake Engineering Research Center, Sponsor: National Science Foundation, Washington, DC, 303p.
- Malley, J.O. and Popov, E.P. (1984), "Shear Links in Eccentrically Braced Frames," *Journal of Structural Engineering*, Vol. 110, No. 9, pp. 2275–2295.
- Marshall, K. (2013), "Earthquake Induced Eccentrically Braced Frame Link Fracture in the Christchurch Hospital Parking Garage," Master's Thesis, University of California, Davis.
- Merovich, A.T., Nicoletti, J.P. and Hartle, E. (1982), "Eccentric Bracing in Tall Buildings," *Journal of the Structural Division*, Vol. 108, No. ST-9, pp. 2066–2080.
- Popov, E.P., Kasai, K. and Engelhardt, M.D. (1987), "Advances in Design of Eccentrically Braced Frames," *Bulletin of the New Zealand National Society for Earthquake Engineering*, Vol. 20, No. 1, pp. 22–29.

- Ricles, J.M. and Popov, E.P. (1987b), "Dynamic Analysis of Seismically Resistant Eccentrically Braced Frames," *Report: UCB/EERC-87/07*, California University, Richmond. Earthquake Engineering Research Center, Sponsor: National Science Foundation, Washington, DC; American Iron and Steel Institute, Washington, DC, 364p.
- Ricles, J.M. and Popov, E.P. (1987a), "Experiments on Eccentrically Braced Frames with Composite Floors," *Report: UCB/EERC-87/06*, California University, Richmond. Earthquake Engineering Research Center. Sponsor: National Science Foundation, Washington, DC; American Iron and Steel Institute, Washington, DC, 330p.
- Roeder, C.W. and Popov, E.P. (1978), "Eccentrically Braced Steel Frames for Earthquakes," *Journal of the Structural Division*, ASCE, Vol. 104, No. 3, pp. 391–412.
- Roy, Y.A., and Dodds R.H, Jr. (2001), "Simulation of Ductile Crack Growth in Thin Aluminum Panels Using 3-D Surface Cohesive Elements," *International Journal of Fracture*, Vol. 110, No. 1, pp. 21–45.
- Simulia (2012), "Abaqus Documentation," <http://www.3ds.com/products-services/simulia/support/documentation/>.